Superconducting and Conventional Electromagnetic Launch System for Civil Aircraft Assisted Take-off

Luca Bertola, Tom Cox, Pat Wheeler, Seamus Garvey
Institute for Aerospace Technology
The University of Nottingham
Nottingham, UK

***Abstract*— This paper compares three possible linear motor topologies for an electromagnetic launch system to assist civil aircraft take-off. Assisted launch of civil aircraft has the potential of reducing the required runway length, reducing noise and emissions near airports and improving overall aircraft efficiency through reducing engine thrust requirements. A comparison is made of practical designs of a linear induction motor, a linear permanent magnet synchronous motor and a superconducting linear synchronous motor to propel the A320-200 aircraft. The machine design requirements are established considering aerodynamic and engine performance and allow the aircraft to safely complete the take-off procedure. Analytical design of conventional synchronous and asynchronous linear motor will be compared with finite element analysis. A superconducting synchronous motor design is also considered, accounting for full system losses including the cryocooler power requirement and the mechanical & design constraints necessary for the cooler and the superconducting coils.**

Keywords—Electromagnetic Launch, Linear Induction Motor, Linear Permanent Magnet Synchronous Motor, Linear Superconducting Synchronous Motor, Civil Aircraft

I. INTRODUCTION

The engine size of modern aircraft is principally determined by take-off conditions, since initial acceleration requires maximum engine power. An Electromagnetic Launch (EML) system could provide some or all of the entire energy required at the launch stage so that the engine power requirement, ground level emissions and fuel use may be significantly reduced. So far, EML has been adopted only for military applications to replace steam catapults on the deck of aircraft carriers [1], [2]. This paper will describe the application of EML to propel civil aircraft on the runways of modern airports as shown in Figure 1, and will compare three different topologies that can be exploited for this purpose.

A linear induction motor (LIM), a linear permanent magnet synchronous motor (LPMSM) and a superconducting linear synchronous motor (SCLSM) design have been compared for military EML systems in [3]. Stumberger considered only two possible stator windings distributions with either 1 or 0.5 phase per pole as viable design solutions for LPMSM. However fractional-slot windings can be exploited to drastically reduce the motor cogging force. The distribution algorithm in [4] will be adopted to select the winding sequence that produces the highest performance for

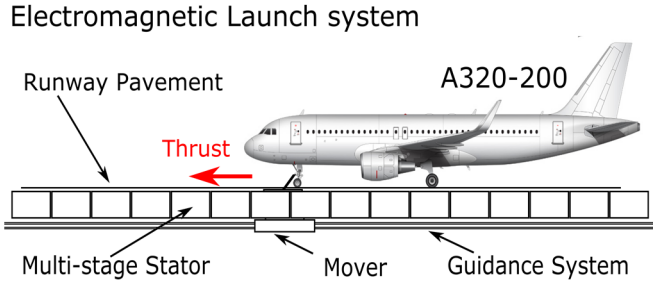

Figure 1: Schematic of an EML system for the aircraft A320-200

a given number of slots and poles. The secondary of the LIM in [3] is made out of copper while aluminum can be exploited slightly reducing the electromagnetic performance, but significantly decreasing the mover weight to obtain the maximum kinetic energy transfer to the aircraft. The bulk YBCO superconducting material for SCLSM in [3], is replaced by magnesium diboride (MgB_2) superconducting coils. MgB_2 has a relatively low transition temperature (39 K) with respect to other high temperature superconducting materials, but Stumberger in [3] concluded that YBCO are not suitable for EML launch unless the temperature is reduced to 40 K. MgB_2 was selected for its better mechanical properties, lower bending radius, round cable availability and lower cost.

The effects of the MMF fundamental harmonic on the performance of synchronous and asynchronous linear motors with the same stator geometry have been presented in [5]. However the performance of LIMs tends to increase with longer pole pitch while the synchronous motor performance is improved by short pole pitch. Moreover the high harmonic content of the magnetic wave in the airgap of concentrated winding distribution is not suitable for a LIM, as the torque contribution from all harmonics must be considered. A comparison cannot be made on the same stator geometry without significantly penalizing one of the topologies under investigation. Therefore this paper compares LIM, LPMSM and SCLSM for a civil aircraft launch system with different stator geometry, each one optimized to achieve the same thrust level and end speed.

The impact of secondary harmonics, skin effect, flux fringing and edge effect are considered in the design procedure of LIM. The decrease of SCLSM's performance due to cryocooler efficiency is evaluated considering the cooler configuration present in [6]. The machines were design to fulfil the requirements reported in Table 1.

TABLE 1: LIST OF REQUIREMENTS FOR THE AIRCRAFT A320-200 LAUNCHER

Requirements	A320 Launch
Aircraft mass	73500 kg
Take-off speed	85.73 m/s
Acceleration	0.60 g
Peak Thrust	502.9 kN
Runway length	624 m
Take-off time	14.57 s
Minimum cycle time	90 s

The end-speed design requirement for the civil aircraft launcher was established considering a factor 1.15 with respect to the speed at which the aircraft detaches. The mover of the catapult disconnects when the aircraft reaches the nose rotation speed. The nose rotation speed was determined considering the aerodynamic performances which allow the aircraft to take-off safely in one engine inoperative conditions. The engines performance decrease at high ambient temperatures was considered as well to accurate estimate the most demanding thrust and end-speed the catapult needs to cope with.

The acceleration of 0.6 g was selected to guarantee an appropriate level of comfort to the passengers considering the maximum axial acceleration safety limits established by the American Standard [7]. The peak thrust in Table 1 was computed considering the aerodynamic drag and the friction with the ground at the end of the launch.

II. DESIGN OF SUPERCONDUCTING LINEAR SYNCHRONOUS MOTOR

The proposed electromagnetic launcher has embedded superconducting coils (SCs) that produce the required excitation field. A double-sided configuration has been selected to avoid the generation of normal forces. The track is placed vertically under the runway and is subdivided in sections which are progressively connected to the energy supply as shown in Figure 2. Distributed double layer stator windings were selected to limit the harmonic content of the magnetomotive force and therefore reduce the AC losses in the superconductors.

The mover that is connected to the aircraft undercarriage and detaches at the end of the acceleration is a cryostat which hosts the superconducting coils submerged in liquid hydrogen. Before the launch the cryostat is sealed to avoid any hydrogen leakage. During the launch part of the hydrogen evaporates absorbing the heat coming from the superconducting coils. After each launch the cryostat is refilled with liquid hydrogen to keep the MgB_2 superconductors at the design temperature. This cooling method has been selected to avoid any movable connection with the external refrigeration system and to reduce the number of machine components at cryogenic temperature.

The structure of the cables proposed for the superconducting launcher is very similar to the one adopted by CERN to achieve the world record in transport current in 2014 [8]. Ten cables were implemented and to enforce the field strength some smaller cables were inserted in the spaces available between the main ones as shown in Figure 3.

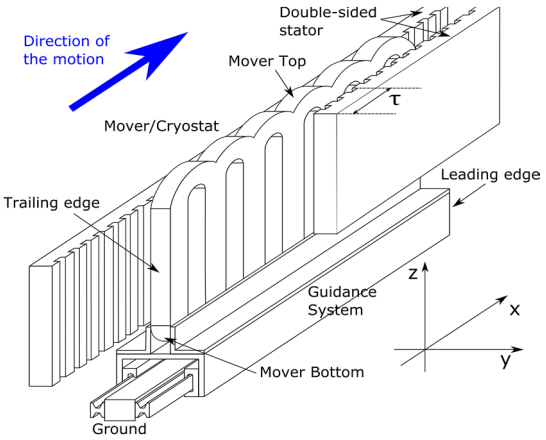

Figure 2: Section of SCLSM for a four pole machine

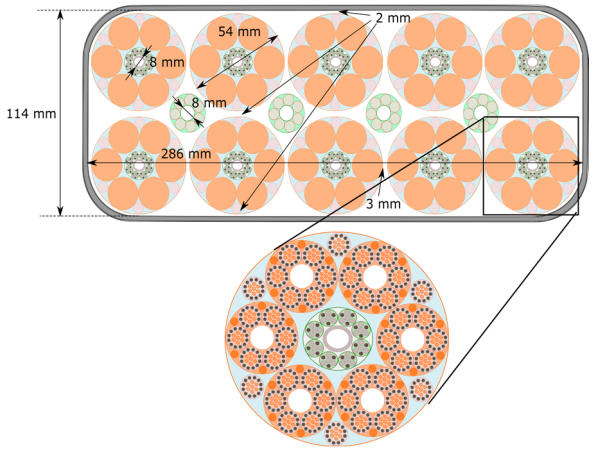

Figure 3: Cross section of the cryostat and of the superconducting cable with relative dimensions

Once all the geometrical properties of the cryostat and of the superconducting cables are defined it is possible to reconstruct the field generated by a single pole and then extend the results to the whole machine taking advantage of the symmetry of the magnetic wave. The flux across a single pole can be compute considering the average magnetic flux density along the stator height as

$$\phi = \frac{1}{h_s}\int_0^{l_s}\int_0^{2\tau}\int_0^{h_s}\vec{B}_y(x,y,z)\,dydxdz \qquad (1)$$

where $\vec{B}_y$ is calculated applying the Biot-Savart's law to all the superconducting filaments that compose the cable in Figure 3. Once the magnetic flux is obtained the stator rated current can be computed from

$$I_s = \frac{2}{3}\frac{\tau}{\pi}\frac{F_x}{2\phi \cdot k_{w1}N_1}. \qquad (2)$$

2ϕ is the magnetic flux produced by the two stators, k_{w1} is the winding factor, N_1 is the number of turns per phase and I_s is the current per turn. The current circulating in the stator coils generates a magnetic field whose fundamental harmonic is synchronized to the mover speed by the control system. The stator windings also generate a series of

secondary harmonics with different intensities, synchronous speeds and frequencies. Multi-Layer Theory (MLT) [9] is applied to reconstruct the field generated by the stator windings and its harmonic content. Since the speeds of the secondary harmonics are different from the fundamental, they are unsynchronized with the motion. The alternating field of the secondary harmonics causes losses that can be classified as eddy current losses, hysteresis losses and coupling losses.

Even though these losses generate heat, the liquid hydrogen stored in the cryostat is capable of removing the heat preventing MgB_2 quenching. The total heat losses are used to size the cryocooler and to determine its power requirement. The cryogenic refrigeration system under consideration is a Reverse-Brayton cryocooler (RBC) for aerospace application which output power can be computed as

$$Q_c = P_{AC} t_{to} / (2t_c), \tag{3}$$

where P_{AC} is the peak alternating current loss, 2 comes from the integration of the AC losses as linearly increasing function, t_{to} is the take-off time and t_c is the minimum time between two consecutive launches (cycle time in Table 1). The model of the cryocooler for aerospace application predicts an efficiency η_c of 1.35% when water at environmental temperature is used as heat sink. The cryocooler input power can be easily computed from the efficiency and the output power as Q_c/η_c.

III. Design of Linear Induction Motor

A multistage, double-sided and long primary (active guideway) LIM was adopted for EML. The double-sided configuration was chosen to have little to no normal force between stators and mover. With an active guideway there is no need to transfer power on board the mover. The multistage configuration in Figure 1 allows the power supply to feed each stage separately. Distributed windings along with the proper coil pitch and number of slot per pole per phase are selected in order to get a MMF as close as possible to a sinusoidal distribution. In each stage the distributed windings are fed with increasing frequency while the reaction plate is moving in order to maintain an optimal thrust and minimal slip level. The reaction plate is made out of aluminum for its low density, high strength and high electrical conductivity. The double-sided stator and the guidance system are similar to those represented in Figure 2, while the mover is shown in Figure 4.

The complexity of the induction machine requires a numerical algorithm to size the motor considering requirements, constraints and input power minimization. The numerical approach that was adopted is based on the sensitivity analysis of the system which is particularly suitable to identify the way a model with a large number of parameters "senses" the variations of some design inputs. This numerical method is performed by running a mathematical algorithm a large number of times for each combination of the input variables. The numerical approach aims to minimize the input power P_i that can be expressed as

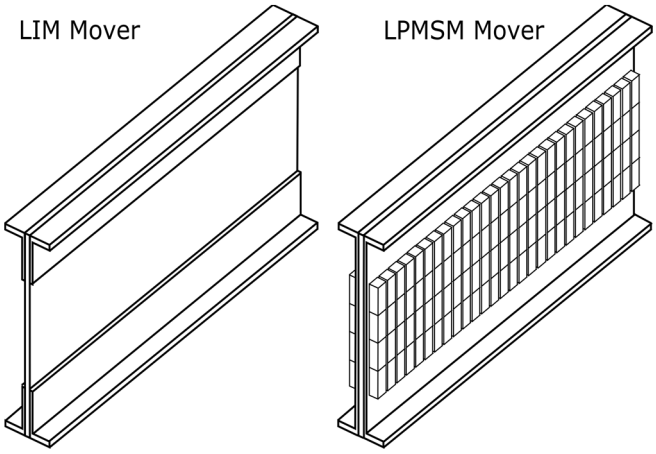

Figure 4: Linear induction motor and linear PM synchronous motor movers

$$P_i = \frac{P_o}{\eta \cos\phi}. \tag{4}$$

where P_o is the output power and the efficiency η and the power factor $\cos\phi$ can be computed as

$$\eta = \frac{F_x V_{end}}{F_x V_{end} + P_{core} + 3R_1 {I_1}^2 + 3R_2 {I_2}^2} \tag{5}$$

$$\cos\phi = \frac{\frac{F_x V_{end}}{\eta}}{\sqrt{\left(\frac{F_x V_{end}}{\eta}\right)^2 + \left\{3\omega_1\left[L_{1l}{I_1}^2 + L_m\left({I_1}^2 - {I_2}^2\right)\right]\right\}^2}} \tag{6}$$

where F_x and V_{end} are the thrust and speed requirements in Table 1, P_{core} is the core loss, R_1 and R_2 the primary and secondary resistance respectively, I_1 and I_2 the primary and secondary current respectively, ω_1 the primary angular velocity and L_{1l} and L_m the leakage and magnetization inductance respectively.

The geometrical features determined by the sensitivity analysis were implemented in a finite element analysis (FEA) software and in an analytical model. The dynamic behavior of the machine was simulated using the LIM d-q equivalent circuit. The classic equivalent circuit for a rotary induction machine was modified to take into account specific LIM phenomena like end-effect and edge effects.

$$\overline{V_1} = R_1 \cdot \overline{I_1} + \frac{\partial \overline{\Psi_1}}{\partial t} + j \cdot \omega_1 \cdot \overline{\Psi_1} \tag{7}$$

$$0 = R_2 \cdot \overline{I_2} + \frac{\partial \overline{\Psi_2}}{\partial t} + j \cdot (\omega_1 - \omega_r) \cdot \overline{\Psi_1} \tag{8}$$

$$0 = R_e \cdot \overline{I_e} - \frac{\partial \overline{\Psi_m}}{\partial t} - j \cdot \omega_1 \cdot \overline{\Psi_m} \tag{9}$$

$$\overline{\Psi_1} = L_{1l} \cdot \overline{I_1} + L_m \cdot (1 - k_e) \cdot \overline{I_m} \tag{10}$$

$$\overline{\Psi_2} = \overline{\Psi_m} \tag{11}$$

$$\overline{\Psi_m} = L_m \cdot (1 - k_e) \cdot \overline{I_m} \tag{12}$$

$$\omega_r = \frac{\pi}{\tau} \cdot v_s \cdot (1 - s) \tag{13}$$

$$\overline{I_1} = I_{1d} + jI_{1q} \tag{14}$$

$$\overline{I_2} = I_{2d} + jI_{2q} \tag{15}$$

$$\overline{I_m} = I_{md} + jI_{mq} \tag{16}$$

$$\overline{I_e} = I_{ed} + jI_{eq} \tag{17}$$

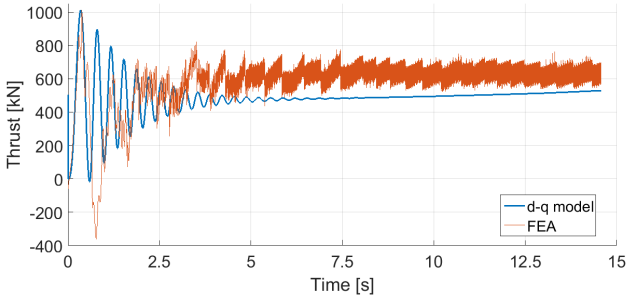

Figure 5: Comparison between analytical and FEA results

The comparison between the thrusts computed by analytical and FEA result is shown in Figure 5. The gap between the thrust profile computed by FEA and the one determined analytically is mainly due to the fact that the 2D finite element simulation does not consider three dimensional effects like edge-effects, end-coil flux leakage and Joule losses which instead are considered in the analytical model. The numerical investigation of these phenomena of LIM with FEA requires a 3D simulation which usually requires vast computational resources.

The FEA accurately predicts the behavior of the machine at the beginning of the launch in Figure 5 where the thrust becomes negative for a short time when the mover exceeds the synchronous speed. The oscillations of the FEA's thrust are due to the transition effect between one stage and the next one, while the oscillations of the analytical method are mainly due to the numerical integration of the differential equation of d-q model.

IV. Design of Linear Permanent Magnet Synchronous Motor

The machine is a double-sided long stator LPMSM with fractional slot pitch tooth windings fed with a common increasing frequency. The armature was designed accounting for minimum use of permanent magnet materials to give a cost effective, low weight solution for a large number of launches. The mover with surface mounted PM on both sides is shown in Figure 4. The fractional slot pitch or concentrated winding configuration can be more efficient for a long segmented stator for EM launch, since transition effects between segments can be reduced. Such a winding layout is easier to manufacture, less expensive and more robust with fewer connections than a distributed one and has shorter end-windings with consequent reduced Joule losses.

Sensitivity analysis has been adopted for the selection of the motor parameters to implement in the FEA and in the analytical model of the LPMSM. As for LIM, the sensitivity analysis algorithm aims to minimize the input power P_i calculate as shown in eq. (4).

The analytical model of LPMSM is based on the Multi-layer theory (MLT) which was applied in [9] and [10] to describe a single-sided LPMSM. In this study, MLT was applied to compute the magnetizing inductance and the overall PM magnetic flux across the double-sided motor. This method is based on the solution of the Maxwell's equation for a layered structure where the primary current and the magnet's field are replaced by synchronized current

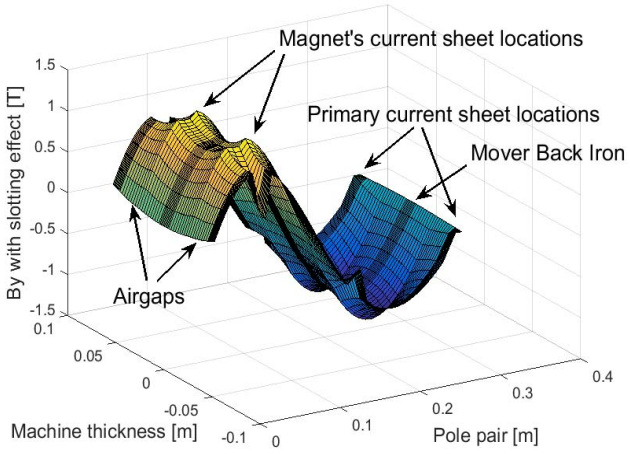

Figure 6: Magnetic field density across the PM motor over a cross section perpendicular to the airgap

sheets. The solution of the Maxwell's equation allows the computation of the magnetic field components as

$$\frac{\partial^2 H_x}{\partial y^2} - \frac{\mu_x \pi^2}{\mu_y \tau^2} H_x = 0 \tag{18}$$

$$H_y = j \frac{\pi}{\tau} \frac{\partial H_x}{\partial y} \tag{19}$$

where μ_x and μ_y are the permeabilities of the stator. The magnetic field density across the machine is determined from the field components as shown in Figure 6.

Once the magnetic field density is known, the magnetic flux across the stator's sides and the back electromotive force can be computed. The inductance of the motor is computed applying the MLT to the primary current sheet after the removal of secondary excitation field.

When cogging forces are treated as disturbances the dq-model of LPMSM can be safely applied. The phasor diagram has been used to represent the dynamic behavior of the machine under operative conditions. In the case of a tooth winding the model reflects the action of the fundamental electromotive force, while other space harmonics are not considered. Indeed, in a synchronous machine the secondary harmonics will have no direct effect on force production, but only cause additional iron losses or even demagnetization. The force acting on mover is calculated as

$$F_x = \frac{3}{2} \frac{\pi}{\tau} \left[\psi_{PM} I_q + \left(L_d - L_q \right) I_d I_q \right] \tag{20}$$

where I_q, I_d are the d-q axis components of the current and L_d, L_q are the d-q inductances. The model provides a good estimation of steady-state and dynamic performance as shown in Figure 7. From Figure 7 it can be observed that the MLT slightly underestimates the thrust at the beginning of the acceleration, but MLT and FEA thrust profiles match at the end of the launch. The FEA model predicts the thrust reasonably well, but the output thrust gradually decreases due to the effects of non-linear iron and of the eddy current losses in the magnets. The thrust predicted by MLT is constant because it assumes linear behavior of the stator

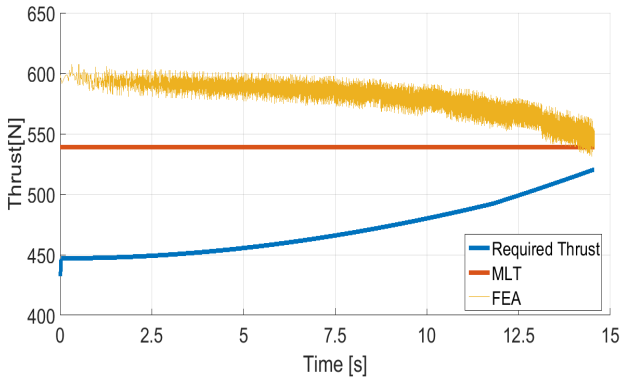

Figure 7: MLT and FEA results comparison

material and it does not consider the effects of secondary harmonics.

V. Comparison

The electromagnetic performances of the three topologies are reported in Table 1. High values of efficiency and power factor have a significant bearing on the viability of this type of system, as these directly affect the size and cost of the power conditioning and energy storage systems.

The mass of the mover has to be as low as possible in order to transfer the major quantity of kinetic energy to the aircraft. LIM has the lightest and simplest mover while SCLSM's secondary is rather heavy even without considering the weight of the pumps needed to force the hydrogen flow through the narrow duct of the cryostat. Moreover the pressure increase due to hydrogen evaporation is not considered here and the cryostat walls thickness and weight may need to increase to accommodate this, even if implementing a pressure regulation valve.

SCLSM has the best electromagnetic performance and requires less power to operate. However, the input power of the cooling system has a great impact on the overall EML system performance. In case the input power of the cryocooler is considered, LPMSM becomes the system with the lowest power demand.

The operating voltages of LIM and LPMSM cannot be easily handled by the current state of the art switching and power conditioning technology. Series connected SiC super GTOs in the range of 10-20 kV and SiC p-IGBTs with 12 kV stopping voltage and switching time of few µs (~ 100 kHz) presented in [11], may be suitable for EML applications. If the peak voltage cannot exceed a predetermined threshold the machine may pass from "constant thrust" mode to "constant power" mode.

Despise the significant complexity and the engineering challenges the superconducting motor has the best electromagnetic performance. The major power loss inside the superconductors is due to the AC losses of the MgB_2 wires. They are caused by the oscillating field of the secondary harmonics which is not synchronized with the motion of the mover. Nevertheless, the efficiency and the electromagnetic performance of the machine is greater than that of the other topologies.

Table 2: Comparison between the performances of LIM, LPMSM and SCLSM with and without cryocooler

	LIM	LPMSM	SCLSM	SCLSM & cooler
Peak Efficiency	0.926	0.989	0.927	0.688
Power Factor	0.586	0.719	0.9998	0.9999
End-Thrust [kN]	523.8	517.6	546.0	546.0
Input Power [MW]	82.78	62.40	50.50	68.06
Current (RMS) [A]	1086	1192	1475	1475
Peak Voltage [kV]	25.41	17.29	11.26	11.26
Armature mass [kg]	868.9	2498.2	7318	7318

Table 3: Comparison between key parameters of LIM , LPMSM and SCLSM

	LIM	LPMSM	SCLSM
Pole pitch [mm]	600	154	500
Stack width [mm]	2000	2000	2000
Airgap length [mm]	7	7	150
Magnet thickness [mm]	-	40.7	540
Magnet length [mm]	-	139	-
Slot pitch [mm]	50	120	167
Slot width [mm]	37.5	30	67
Slot height [mm]	5.1	7.0	10
Poles pair	3	14	4
Slot per pole per phase	4	3/7	1
Current density [A/mm^2]	50	50	47.2
Thrust density [Pa]	70560	59908	68246

VI. Conclusion

However, when the input power of the cryocooler required to keep the superconductors at cryogenic temperature is considered, the efficiency of the overall superconducting system significantly reduces. When the cooling power is taken into account the input power of SCLSM exceeds the one of LPMSM. It may be concluded that LPMSM are more convenient than SCLSM from the input power point of view, but they need a higher voltage and a larger power conditioning system due to the additional reactive power.

The LIM based design may still be attractive for the simplicity of the mover which does not involve expensive material and particular engineering challenges. However the low power factor imposes high operating voltages and requires a high input power.

Acknowledgment

The research leading to these results has received funding from the People Programme (Marie Curie Actions) of the European Union's Seventh Framework Programme (FP7/2007-2013) under REA grant agreement no 608322.

References

[1] K. Lentijo, G. Bellamy, J. Watson, K. Flint, "Launch and Recovery using the EMKIT System," ed: Amercian Society of Naval Engineer 2010.

[2] G. Atomics. (2014, October). *EMALS*. Available: http://www.ga.com/emals

[3] G. Stumberger, D. Zarko, M. T. Aydemir, T. A. Lipo, "Design of a Linear Bulk Superconductor Magnet Synchronous Motor fo Electromagnetic Aircraft Launch Systems," *IEEE Transaction on Applied Superconductivity,* vol. 14, pp. 54-62, March 2004.

[4] L. Bertola, T. Cox, P. Wheeler, S. Garvey, H. Morvan, "Electromagnetic Launch Systems for Civil Aircraft Assisted Take-off," *Archive of Electrical Engineering,* vol. 64, pp. 543-554, 2015.

[5] Gorazd Stumberger, Damir Zarko, Mehemet Timur Aydemir, Thomas A. Lipo, "Design and Comparison of Linear Synchronous Motor and Linear Induction Motor for Electromagnetic Aircraft Launch System," presented at the Electrical Machines and Drives, 2003.

[6] F. Berg, J. Palmer, L. Bertola, P. Miller, G. Dodds, "Cryogenic system options for a superconducting aircraft propulsion system," *IOP Conference Series: Materials Science and Engineering,* vol. 101, 2015.

[7] ASTM, "Standard Practice for Design of Amusement Rides and Devices," vol. F2291-13, ed, 2014.

[8] W. Goldacker, S. I. Schlachter, "HTS and MgB_2 cables for application in energy technology and magnets," Karlsruhe Institute of Technology2011.

[9] Z. Deng, I. Boldea, S. A. Nasar, "Fields in Permanent Magnet Linear Synchronous Machines," *IEEE Transaction on Magnetics,* vol. 2, pp. 107-112, 1986.

[10] Z. Deng, I. Boldea, S. A. Nasar, "Forces and Parameters of Permanent Magnet Linear Synchronous Machines," *IEEE Transaction on Magnetics,* vol. 1, pp. 305-309, 1987.

[11] A. Agarwal, Q. Zhang, A. Burk, R. Callanan, "Prospects of bipolar power devices in silicon carbide," in *34th Annual Confrence of IEEE Industrial Electronics 2008*, 2008, pp. 2879-2884.